Available online at www.sciencedirect.com
SCIENCE DIRECT®
Journal of Sound and Vibration 281 (2005) 537–564
JOURNAL OF SOUND AND VIBRATION
www.elsevier.com/locate/jsvi

Nonlinear dynamics of cable stays. Part 1: sinusoidal cable support excitation

C.T. Georgakis*, C.A. Taylor

Department of Civil Engineering, Earthquake Engineering Research Centre, University of Bristol, Queens Building, University Walk, Bristol BS8 1TR, UK

Received 10 August 2001; accepted 27 January 2004
Available online 30 September 2004

Abstract

An extensive behavioural study of cable vibrations, induced by sinusoidal cable-plane structural vibrations, is presented. Nonlinear equations of motion are formulated for a hanging cable with a small sag-to-span ratio. The effects of sinusoidal cable support displacements, with abrupt and gradual transients, are studied. Cable in-plane and out-of-plane displacements are generated through multiple shape-function analyses. Previously observed regions of large amplitude cable vibrations, in the excitation amplitude/frequency parameter plane and for sinusoidal cable end displacements, are verified and new regions of response instability are found. In addition, regions within the parameter plane are characterised as periodic, quasi-periodic or chaotic. The effects of changes in initial cable conditions are examined and differences in maximum displacement amplitudes are found and compared to those found from a *zero*-initial-condition sinusoidal support excitation. For specific excitation amplitude/frequency parameter pairs, 'cable stiffening' is observed. Throughout the analysis, maximum cable stresses are calculated and found to be less than those required for material yielding. The significance of a cable-support interaction is briefly discussed.

*Corresponding author. Skovagervej 7, Holte, DK-2840 Denmark.
E-mail address: cg@force.dk (C.T. Georgakis).

0022-460X/$ - see front matter © 2004 Elsevier Ltd. All rights reserved.
doi:10.1016/j.jsv.2004.01.022

Nomenclature

w_o^c	mid-span sag of cable at rest
l	total length of cable
$U_x(x,t)$, $U_y(x,t)$, $U_z(x,t)$	dynamic cable displacement components in three dimensions
t	dimensional time
$\bar{t}$	nondimensional time
x	distance along the cable
$\bar{x}$	nondimensional distance along the cable
E	material modulus of elasticity
A	cross-sectional area of cable
g	gravitational acceleration
θ	angle of inclination of the cable
D	cable diameter
H_k	kinetic energy
H_σ	strain energy
H_σ^{static}	static strain energy
$H_\sigma^{\text{dynamic}}$	dynamic strain energy
H_g	work done by gravity
H_g^{dynamic}	dynamic gravitational energy
H_g^{static}	gravitational potential energy
μ	mass per unit length of cable
$C(x)$	static equilibrium cable curvature
$N(x)$	initial cable tension
N_c	cable tension at mid-span
$\varepsilon(x,t)$	dynamic cable strain
$\varepsilon_d(x,t)$	dynamic component of dynamic strain $\varepsilon(x,t)$
$\varepsilon_d(\bar{t})$	total nondimensional time dependant dynamic strain of cable
u, u_x, u_y, u_z	nondimensional cable displacements
v_t^2	transverse wave propagation speed
v_l^2	longitudinal wave propagation speed
$\Delta(t)$	vertical cable support displacement
$\dot{\Delta}(t)$	vertical cable support velocity
$\ddot{\Delta}(t)$	vertical cable support acceleration
$\Delta_{\max}$	maximum vertical cable support displacement
$\delta, \delta(\bar{t})$	nondimensional vertical cable support displacements
$\dot{\delta}, \dot{\delta}(\bar{t})$	nondimensional vertical cable support velocity
$\ddot{\delta}, \ddot{\delta}(\bar{t})$	nondimensional vertical cable support acceleration
$f_{yi}(\bar{x}), f_{zi}(\bar{x})$	in-plane and out-of-plane cable shape functions
$\psi(\bar{x})$	support displacement shape function
n	total number of shape functions used
i	shape function number 1,2,3,…
ω_{yi}, ω_{zi}	linear in-plane and out-of-plane cable circular frequencies
ω_1^{nl}	in-plane first circular frequency accounting for cable sag
ω_k	cable's modal circular frequencies
Ω	cable support excitation frequency
d_y, d_z	in-plane and out-of-plane cable damping coefficients
ξ_y, ξ_z	in-plane and out-of-plane cable damping ratios
d_g^y, d_g^z	in-plane and out-of-plane damping
d_c^y, d_c^z	critical in-plane and out-of-plane damping
ξ_{pk}	aerodynamic parallel to wind damping ratios of cable
ξ_{nk}	aerodynamic normal to wind damping ratios of cable
β	nondimensional cable support displacement level parameter
ρ	density of air
C_d	cable drag coefficient
V	wind velocity
$\sigma_y, \sigma_{\max}$	cable material yield stress and maximum observed stress respectively

1. Introduction

The study of cable vibrations is of considerable interest, as cables on many cable-stayed bridges, telecommunications masts and other similar structures frequently exhibit large amplitude in-plane

and out-of-plane vibrations. Most small to medium amplitude cable vibrations can be explained as wind or wind-rain/ice-induced through flutter, vortex shedding, galloping and other similar mechanisms [1–4]. Larger amplitude vibrations, although, are not well explained through these mechanisms and may, more justifiably, be attributed to parametric support excitation. Yamaguchi and Fujino [5] have reported the parametric excitation of cable-stays, induced by the artificial excitation of a prototype cable-stayed bridge deck, under particular conditions.

Irvine and Caughey [6,7] have studied the free vibrations of cables in detail, using linear equations of motion. Takahashi and Konishi [8,9], who managed to locate regions of instability, in which cables exhibit large in-plane and out-of-plane displacements, have studied the effects of sinusoidal time-varying cable support displacements using nonlinear equations of motion. Fujino et al. [10,11], Lilien and Pinto da Costa [12], Pinto da Costa et al. [13] and Perkins [14] have successfully extended this work to include variations of the angle at which the support excitation is applied, the damping of the cables, the method of analysis, and the detailed explanation of the cable dynamics.

In all of the theoretical studies mentioned above, a cable of finite length with a uniformly distributed mass and a relatively small sag-to-span ratio is examined. The cable is placed between two supports at the same or different levels. The derived nonlinear equations of motion consider the parabolic shape of the cable under the influence of gravity. Three partial differential equations (PDEs), explaining the parametric excitation of the cable along its axis and in its in-plane and out-of-plane components, are transformed into ordinary differential equations (ODEs) using the Galerkin or other similar de-coupling methods [7–15]. The PDEs are de-coupled when the acceleration term of the equation of motion, describing the cable's along-axis excitation, is equated to zero. Finally, approximate solutions for the ODEs are found, and the results are compared to observations of actual and experimental cable vibrations.

The aim of the present study is to provide further insights into the dynamics of cables subjected to sinusoidal support excitation. In addition, a methodology is developed for the examination of in-plane sinusoidal support excitations, resulting from both along cable and normal to cable support displacements. The parametric study of a cable's dynamics through traditional finite element analyses is laborious and therefore is not suited to detailed and rigorous investigations. However, the analytical methodology presented here is relatively simple and permits large parameter spaces to be explored with modest computing resources.

All of the presented analyses were performed using readily available software packages [17]. As with previous works, the nonlinear equations of motion of the hanging cable are formulated using the Galerkin method to provide a system of ODEs that can easily be implemented into numerical integration tools [16]. Several shape-functions, for both in-plane and out-of-plane vibrations of an example cable, are used and the significance of their inclusion is described. Sub-regions within the parameter plane are defined as periodic, quasi-periodic or chaotic, and amplitudes of cable in-plane and out-of-plane displacements are assessed, as is the importance of structural and aerodynamic damping. The effects of initial displacements on the cable are examined and the results are compared to those found from *zero*-initial-condition cable analyses. During the analyses, the cable material stresses were monitored continuously, as it was assumed throughout the analyses that the cable behaves elastically.

Past investigators have assumed that a cable's support excitation is predetermined, i.e. that the cable can have no effect on its support throughout its excitation. This assumption has been carried

through to this work, but it must be noted that it can only hold true if the mass of the structure at the end of the cable is, for all practical purposes, 'infinitely' greater than the mass of the cable in question. This assumption cannot be made without defining appropriate structural mass to cable mass ratios at which the cable has no or little effect on its support. For the purposes of this paper, it will be assumed that the mass of the cable-supported structure is 'infinitely' greater than the mass of the cable in question. The effects of a change to these ratios have been examined by Georgakis [17] and will be discussed in a subsequent paper.

It is also usually assumed that *one* or *two* shape-functions are sufficient for the accurate analysis of the dynamic response of cables through the numerical integration of a cable's system of ordinary differential equations of motion. This is not always true and, as will be shown, more shape-functions are generally needed for an accurate cable response analysis.

2. Formulation of nonlinear equations of motion

2.1. Model assumptions

Before the equations can be derived a theoretical inclined cable model under the influence of gravity, where the maximum static deflection or sag of the cable is small and less than 1/100th of the total cable length, l (Fig. 1), will be assumed. The cable material is assumed to behave elastically. The cable will displace statically in a near-parabolic manner under the influence of gravity. Thus, $w_0^c/l < 1/100$, where w_0^c is the static sag at mid-length of the cable. This restriction is necessary, so that the PDEs can later be decoupled, by equating the axial acceleration to zero. This can be done, as the longitudinal wave propagation speed is much greater than the equivalent in-plane and out-of-plane wave propagation speeds. The cable is inclined at an angle θ and is fixed at one end. The cable is excited in-plane at one end and the displacement at that end at time t is denoted by $\Delta(t)$. When the end of the cable is displaced dynamically, the global response of the cable at any point, x, along the cable is time dependent and denoted as $U(x, t)$. $U(x, t)$ is composed of three displacement components $U_x(x, t)$, $U_y(x, t)$, $U_z(x, t)$, which describe the displacement of the cable along its axis, in-plane and out-of-plane, respectively. For simplicity, the dependency (x, t) of these components will be omitted in the subsequent equations.

2.2. Derivation of equations

Following Refs. [14,15], the equations that govern the global response of a cable can be obtained by applying Hamilton's energy principle. That is

$$\int_{t_0}^{t_1} [H_k + H_g]\,\mathrm{d}t = \int_{t_0}^{t_1} H_\sigma\,\mathrm{d}t, \tag{1}$$

where H_k is the cable's kinetic energy, H_σ is the cable's strain energy and H_g is the work done by gravity.

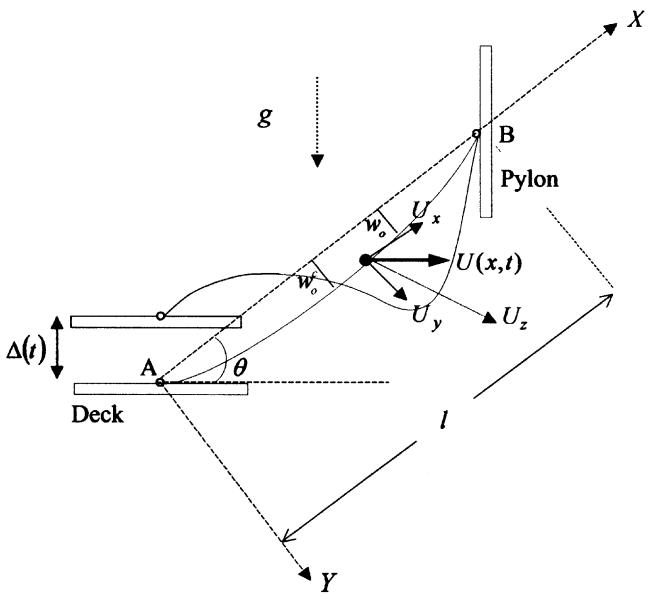

Fig. 1. Motion of a single hanging cable with end support displacement.

The kinetic energy of the cable is

$$H_k = \int_0^l \tfrac{1}{2}\mu \left[\left(\frac{\partial U_x}{\partial t}\right)^2 + \left(\frac{\partial U_y}{\partial t}\right)^2 + \left(\frac{\partial U_z}{\partial t}\right)^2 \right] \mathrm{d}x, \tag{2}$$

where μ is the mass per unit length of the cable.

The cable is assumed to be a homogeneous elastic continuum that will undergo uniform axial extensions along its centre line. This finite-strain description leads to the nonlinear strain–displacement relationship:

$$\varepsilon(x,t) = \frac{N(x)}{EA} + \frac{\partial U_x}{\partial x} - C(x)U_y + \frac{1}{2}\left[\left(\frac{\partial U_x}{\partial x} - C(x)U_y\right)^2 + \left(\frac{\partial U_y}{\partial x} + C(x)U_x\right)^2 + \left(\frac{\partial U_z}{\partial x}\right)^2 \right], \tag{3}$$

where $\varepsilon(x,t)$ is the total strain of the cable in its final dynamic configuration, $C(x)$ is the curvature of the cable in its static equilibrium position, and $N(x)$ is the cable's initial tension. E denotes the cable material's modulus of elasticity, and A the cross-sectional area of the cable. From this it can be seen that the cable's strain–displacement relationship is comprised of static (non time-dependant) and dynamic (time-dependant) components. Thus, the cable's strain energy is described as

$$H_\sigma = H_\sigma^{\text{static}} + H_\sigma^{\text{dynamic}}, \tag{4}$$

where

$$H_{\sigma}^{\text{dynamic}} = \int_0^l \left[N(x)\varepsilon_d(x)^2 + \tfrac{1}{2}EA\varepsilon_d(x)^2\right]\mathrm{d}x \tag{5a}$$

and

$$\text{dynamic strain} = \varepsilon_d(x,t) = \frac{\partial U_x}{\partial x} - C(x)U_y + \frac{1}{2}\left[\left(\frac{\partial U_x}{\partial x} - C(x)U_y\right)^2 + \left(\frac{\partial U_y}{\partial x} + C(x)\cdot U_x\right)^2 + \left(\frac{\partial U_z}{\partial x}\right)^2\right] \tag{5b}$$

and the strain energy at equilibrium,

$$H_{\sigma}^{\text{static}} = \int_0^l \left[\tfrac{1}{2}\varepsilon_s(x)N(x)\right]\mathrm{d}x \tag{6a}$$

and

$$\text{static strain} = \varepsilon_s(x) = \frac{N(x)}{EA}. \tag{6b}$$

The work done by gravity will be

$$H_g = H_g^{\text{static}} + H_g^{\text{dynamic}}, \tag{7}$$

where H_g^{static} is the gravitational potential energy at static equilibrium and $H_g^{\text{static}} = H_{\sigma}^{\text{static}}$. Also,

$$H_g^{\text{dynamic}} = -\int_0^l \mu g\left[U_x \sin\theta + U_y \cos\theta\right]\mathrm{d}x, \tag{8}$$

where θ is the angle of inclination of the component U_x with respect to the horizontal.

Substituting Eqs. (2)–(8) into Hamilton's energy Eq. (1) and integrating by parts the equations of motion in three components are derived:

Component U_x:

$$\frac{\partial}{\partial x}\left[(N(x) + EA\varepsilon_d(x,t))\left(1 + \frac{\partial U_x}{\partial x} - C(x)U_y\right)\right] - \left[(N(x) + EA\varepsilon_d(x,t))\left(C(x)\frac{\partial U_y}{\partial x} + C(x)^2U_x\right)\right] - \mu g\sin\theta = \mu\frac{\partial^2 U_x}{\partial t^2}. \tag{9}$$

Component U_y:

$$\frac{\partial}{\partial x}\left[(N(x) + EA\varepsilon_d(x,t))\left(\frac{\partial U_y}{\partial x} + C(x)U_x\right)\right] + \left[(N(x) + EA\varepsilon_d(x,t))\left(C(x) + C(x)\frac{\partial U_x}{\partial x} - C(x)^2U_y\right)\right] - \mu g\cdot\cos\theta = \mu\frac{\partial^2 U_y}{\partial t^2}. \tag{10}$$

Component U_z:

$$\frac{\partial}{\partial x}\left[(N(x)+EA\varepsilon_d(x,t))\left(\frac{\partial U_z}{\partial x}\right)\right]=\mu\frac{\partial^2 U_z}{\partial t^2}. \tag{11}$$

As described in Ref. [7], the nonhomogeneous terms in Eqs. (9)–(11) disappear for static equilibrium, and the equilibrium curvature, $C(x)$, and tension, $N(x)$, become

$$C(x)=\frac{\mu g N_c}{N_c^2+\left[\mu g\left(x-l/2\right)\right]^2}\cos\theta, \tag{12}$$

$$N(x)=\sqrt{N_c^2+\left[\mu g(x-l/2)\right]^2}, \tag{13}$$

where N_c is the static equilibrium tension at mid-span of the cable.

Because N_c in most cable-supported structures is much greater than $\mu g(x-l/2)$ it can be assumed that

$$N_c^2+\left[\mu g(x-l/2)\right]^2\cong N_c^2. \tag{14}$$

Thus, Eqs. (12) and (13), with approximation (14), become

$$C(x)=\frac{\mu g}{N_c}\cos\theta \tag{15}$$

and

$$N(x)=N_c. \tag{16}$$

By substituting Eqs. (12) and (13) into Eqs. (9)–(11) and neglecting terms with coefficients of $(\mu g l/N_c)^2$ or smaller, the following dimensionless equations are obtained:

$$\frac{\partial^2 u_x}{\partial \bar{t}^2}=v_l^2\frac{\partial}{\partial \bar{x}}\left\{\frac{\partial u_x}{\partial \bar{x}}-cu_y+\frac{1}{2}\left[\left(\frac{\partial u_y}{\partial \bar{x}}\right)^2+\left(\frac{\partial u_z}{\partial \bar{x}}\right)^2\right]\right\}, \tag{17}$$

$$\frac{\partial^2 u_y}{\partial \bar{t}_2}=\frac{\partial}{\partial \bar{x}}\left(\left(v_t^2+v_l^2\left\{\frac{\partial u_x}{\partial \bar{x}}-cu_y+\frac{1}{2}\left[\left(\frac{\partial u_y}{\partial \bar{x}}\right)^2+\left(\frac{\partial u_z}{\partial \bar{x}}\right)^2\right]\right\}\right)\frac{\partial u_y}{\partial \bar{x}}\right)+cv_l^2\left(\frac{\partial u_x}{\partial \bar{x}}-cu_y\right), \tag{18}$$

$$\frac{\partial^2 u_z}{\partial \bar{t}^2}=\frac{\partial}{\partial \bar{x}}\left(\left(v_t^2+v_l^2\left\{\frac{\partial u_x}{\partial \bar{x}}-cu_y+\frac{1}{2}\left[\left(\frac{\partial u_y}{\partial \bar{x}}\right)^2+\left(\frac{\partial u_z}{\partial \bar{x}}\right)^2\right]\right\}\right)\frac{\partial u_z}{\partial \bar{x}}\right). \tag{19}$$

With the nondimensional quantities being

$$\begin{aligned}&\bar{x}=x/l,\quad \bar{t}=t/(l/g)^{1/2},\quad u=U/l,\quad c=\mu g l/N_c\cos\theta,\\ &v_t^2=N_c/\mu g l\cos\theta=\text{transverse wave propagation speed},\\ &v_l^2=EA/\mu g l\cos\theta=\text{longitudinal wave propagation speed.}\end{aligned} \tag{20a–f}$$

As described before, when the sag-to-span ratio is relatively small, it is assumed that the cable stretches in a *quasi-static* manner [14], due to the fact that the propagation speed for longitudinal

waves greatly exceeds that for transverse waves. Thus, $\ddot{u}_x = 0$, and from Eq. (17)

$$\frac{\varepsilon_d(\bar{x},\bar{t})}{\partial\bar{x}} = \frac{\partial}{\partial\bar{x}}\left\{\frac{\partial u_x}{\partial\bar{x}} - cu_y + \frac{1}{2}\left[\left(\frac{\partial u_y}{\partial\bar{x}}\right)^2 + \left(\frac{\partial u_z}{\partial\bar{x}}\right)^2\right]\right\} = 0. \tag{21}$$

Integration leads to

$$u_x(\bar{x},\bar{t}) = \varepsilon_d(\bar{t})\bar{x} + \int_0^{\bar{x}}\left\{cu_y - \frac{1}{2}\left[\left(\frac{\partial u_y}{\partial\bar{x}}\right)^2 + \left(\frac{\partial u_z}{\partial\bar{x}}\right)^2\right]\right\}\mathrm{d}\bar{x}. \tag{22}$$

The boundary conditions for the cable will be

$$u_x(0,\bar{t}) = -\delta\sin\theta, \quad u_x(l,\bar{t}) = 0, \tag{23}$$

$$u_y(0,\bar{t}) = \delta\cos\theta, \quad u_y(l,\bar{t}) = 0, \tag{24}$$

$$u_z(0,\bar{t}) = u_z(l,\bar{t}) = 0, \tag{25}$$

where

$$\delta = \delta(\bar{t}) = \Delta(\bar{t})/l = \text{nondimensional cable end displacement.} \tag{26}$$

Introducing boundary conditions (23)–(25)

$$u_x(\bar{x},\bar{t}) = -\delta\sin\theta + \varepsilon_d(\bar{t})\bar{x} + \int_0^{1}\left\{cu_y - \frac{1}{2}\left[\left(\frac{\partial u_y}{\partial\bar{x}}\right)^2 + \left(\frac{\partial u_z}{\partial\bar{x}}\right)^2\right]\right\}\mathrm{d}\bar{x}, \tag{27}$$

where

$$\varepsilon_d(\bar{t}) = \delta\sin\theta - \int_0^{1}\left\{cu_y - \frac{1}{2}\left[\left(\frac{\partial u_y}{\partial\bar{x}}\right)^2 + \left(\frac{\partial u_z}{\partial\bar{x}}\right)^2\right]\right\}\mathrm{d}\bar{x}. \tag{28}$$

Note that the dynamic tensile force in the cable is

$$T_d(\bar{t}) = EA\varepsilon_d(\bar{t}) = EA\delta\sin\theta - EA\int_0^{1}\left\{cu_y - \frac{1}{2}\left[\left(\frac{\partial u_y}{\partial\bar{x}}\right)^2 + \left(\frac{\partial u_z}{\partial\bar{x}}\right)^2\right]\right\}\mathrm{d}\bar{x}. \tag{29}$$

With Eq. (27), Eqs (18) and (19) become

$$\frac{\partial^2 u_y}{\partial\bar{t}^2} = \left[v_t^2 + v_l^2\varepsilon_d(\bar{t})\right]\frac{\partial^2 u_y}{\partial\bar{x}^2} + cv_l^2\varepsilon_d(t), \tag{30}$$

$$\frac{\partial^2 u_z}{\partial\bar{t}^2} = \left[v_t^2 + v_l^2\varepsilon_d(\bar{t})\right]\frac{\partial^2 u_z}{\partial\bar{x}^2}. \tag{31}$$

These represent the cable's nonlinear in-plane and out-of-plane equations of motion, respectively.

Eqs. (30) and (31) are consistent only for the previously mentioned assumptions and for relatively low excitation frequencies. This, again, is due to the assumption that the cable stretches in a *quasi-static* manner [14].

The differential equations in their final form can be determined using Galerkin's method in which the in-plane and out-of-plane transverse displacements u_y, u_z can be approximated using separable solutions. These will be of the form

$$u_y(\bar{x},\bar{t}) = \sum_{i=1}^{n} u_{yi}(\bar{t}) f_{yi}(\bar{x}) + \delta \cos\theta \psi(\bar{x}), \tag{32}$$

$$u_z(\bar{x},\bar{t}) = \sum_{i=1}^{n} u_{zi}(\bar{t}) f_{zi}(\bar{x}), \tag{33}$$

where $f_{yi}(\bar{x})$ and $f_{zi}(\bar{x})$ are the in-plane and out-of-plane mode shape functions of the linearised problem, respectively, and where $i = 1, 2, 3\ldots$, again refers to natural modes of the linearised problem and n is the number of shape functions considered. $u_{yi}(\bar{t})$ and $u_{zi}(\bar{t})$ are the generalised coordinates of the in-plane and out-of-plane shape functions. Although, as a result of the effect of added tension due to gravity, the in-plane mode shape functions of a cable will differ from their equivalent out-of-plane mode shapes, here it is assumed that the in-plane mode shape functions are the same as the out-of-plane (Fig. 2). This approximation is suitable here, as actual in-plane and out-of-plane mode shape functions tend to provide similar modal displacements. Thus

$$f_{yi}(\bar{x}) = f_{zi}(\bar{x}) = \sin\frac{i\pi x}{l} = \sin\, i\pi\bar{x}. \tag{34}$$

The selection of the shape function $f_{yi}(\bar{x})$ is not crucial for the calculation of the dynamic response of the cable, as long as an infinite number of shape functions are used in the analyses. The appropriate selection of shape function, although, can lead to a significantly reduced number of required shape functions for a sufficiently accurate analysis. It has been shown that the chosen shape-functions do just that, as they are equivalent to the out-of-plane linearised mode shapes of the cable. For the shape function $\Psi(\bar{x})$, it will be assumed that the cable shape, when considering only the displacement of one end, will be as in Fig. 3. The shape-function, describing the forced displacement, is

$$\psi(\bar{x}) = (1-\bar{x})^2 \tag{35}$$

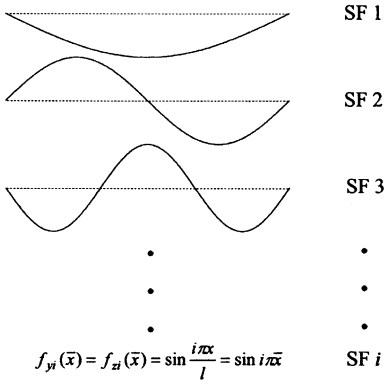

Fig. 2. Shape function used for Galerkin de-coupling.

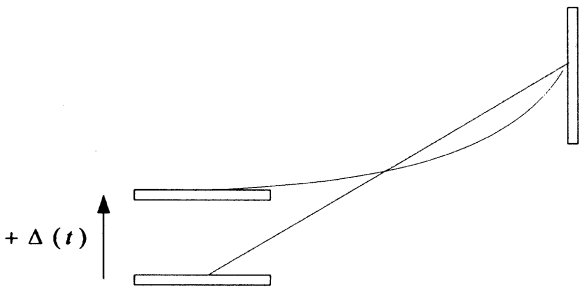

Fig. 3. Cable shape due to positive end displacement.

and is an approximation of the shape that the cable takes, due to a pseudo-static displacement of its end.

Substituting Eqs. (34) and (35) into Eqs. (32) and (33)

$$u_y(\bar{x},\bar{t}) = \delta\cos\theta(1-\bar{x})^2 + \sum_{i=1}^{n} u_{yi}(\bar{t})\sin i\pi\bar{x}, \tag{36}$$

$$u_z(\bar{x},\bar{t}) = \sum_{i=1}^{n} u_{zi}(\bar{t})\sin i\pi\bar{x}. \tag{37}$$

After substitution of Eqs. (36) and (37) into Eqs. (30) and (31), multiplication by $\sin(i\pi\bar{x})$ and integration where needed, the Galerkin method yields a two-degree-of-freedom model with the following system of differential equations for the in-plane and out-of-plane motion of the cable, the ith equations of which are

$$\ddot{u}_{yi}(\bar{t}) + \omega_{yi}^2 u_{yi}(\bar{t}) = F_{yi} \tag{38}$$

and

$$\ddot{u}_{zi}(\bar{t}) + \omega_{zi}^2 u_{zi}(\bar{t}) = F_{zi}, \tag{39}$$

where

$$\omega_{yi}^2 = v_t^2(i\pi)^2, \quad \omega_{zi}^2 = v_t^2(i\pi)^2 = \text{squared linear circular frequencies} \tag{40, 41}$$

and

$$\begin{aligned} F_{yi} = {} & a_{1i}\varepsilon_d(\bar{t})u_{yi}(\bar{t}) + a_{2i}(\beta_1\delta + \beta_2\delta^2 + \beta_3 + \beta_4\delta)u_{yi}(\bar{t}) + a_{3i}(\beta_{5i}\delta + \beta_{6i})u_{yi}^2(\bar{t}) \\ & + a_{3i}(\beta_{7i}\delta + \beta_{8i})u_{zi}^2(\bar{t}) + \frac{2}{n}\gamma_{8i}\ddot{\delta} + a_{3i}\{(\gamma_1+\gamma_2+\gamma_3)\delta + (\gamma_4+\gamma_5+\gamma_6)\delta^2 + \gamma_7\delta^3\} \end{aligned} \tag{42a}$$

when $i = 1$, and

$$\begin{aligned} F_{yi} = {} & a_{1i}\varepsilon_d(\bar{t})u_{yi}(\bar{t}) + a_{2i}(\beta_1\delta + \beta_2\delta^2 + \beta_3 + \beta_4\delta)u_{yi}(\bar{t}) + a_{3i}\big(\beta_{5i}\delta + \beta_{6i}\big)u_{yi}^2(\bar{t}) \\ & + a_{3i}(\beta_{7i}\delta + \beta_{8i})u_{zi}^2(\bar{t}) + \frac{2}{n}\gamma_{8i}\ddot{\delta} \end{aligned} \tag{42b}$$

when $i \neq 1$,

$$F_{zi} = \lambda_{1i}\varepsilon_d(\bar{t})u_{zi}(\bar{t}), \tag{43}$$

where the dynamic strain of the cable is

$$\varepsilon_d(\bar{t}) = \tau_1\delta + (\tau_2 + \tau_5\delta)\sum_{i=1}^{n}\frac{1}{\pi i}u_{yi}(\bar{t})(1 - \cos\,\pi i) + \tau_3\sum_{i=1}^{n}(\pi i)^2u_{yi}^2(\bar{t}) + \tau_3\sum_{i=1}^{n}(\pi i)^2u_{zi}^2(\bar{t}) + \tau_4\delta^2 \tag{44}$$

The undefined coefficients appearing in Eqs. (42)–(44) are defined in Appendix A.

The total dynamic tension of the cable will now be

$$N_t(\bar{t}) = EA\varepsilon_d(\bar{t}) + N_c. \tag{45}$$

Note that the in-plane nonlinear first circular frequency, ω_1^{nl}, due to the sag of the cable, can be found from the following equation [14]:

$$\tan\frac{\omega_1^{\mathrm{nl}}}{2v_t} - \frac{\omega_1^{\mathrm{nl}}}{2v_t} + \frac{(\omega_1^{\mathrm{nl}}v_t)^3}{2v_l^2} = 0. \tag{46}$$

Finally, adding modal damping to Eq. (38) and (39) will lead to

$$\ddot{u}_{yi}(\bar{t}) + \omega_{yi}^2u_{yi}(\bar{t}) = F_{yi} - d_y\dot{u}_{yi}(\bar{t}) \tag{47}$$

$$\ddot{u}_{zi}(\bar{t}) + \omega_{zi}^2u_{zi}(\bar{t}) = F_{zi} - d_z\dot{u}_{zi}(\bar{t}) \tag{48}$$

where

$$d_y = 2\xi_y\omega_{y1} \tag{49}$$

$$d_z = 2\xi_z\omega_{z1} \tag{50}$$

and

$$\xi_y = \frac{d_g^y}{d_c^y} \tag{51}$$

is the ratio of the given in-plane damping to the critical in-plane damping, and

$$\xi_z = \frac{d_g^z}{d_c^z} \tag{52}$$

is the ratio of the given out-of plane damping to the critical out-of-plane damping.

Note that the changes in the angle θ, which occur during dynamic cable vibrations, are small and have a negligible effect on the dynamic behaviour of the cable. Therefore, they have been excluded from the formulation.

3. Numerical integration tools

Numerous cables with various angles of inclination and damping values were analysed by solving the equations of motion of the cables through numerical integration and by finite element modelling. Numerical integration of the equations of motion was done using two different

differential equation solvers, namely DSolver [16] and DynamicsII [18]. Finite Element Modelling (FEM) was achieved using the SOLVIA Finite Element System [19]. The FEM is comprised of ten linked truss elements and has the same geometry, properties and damping as the models solved using the differential equation solvers. The results from both DSolver and DynamicsII are identical and for this reason only the results from DSolver are presented.

4. Selected cable parameters

Due to the infinite number of damping values and angles of inclination that a cable may take, several values were selected to represent typical cables on existing structures, those mainly being cable-stayed bridges. As the equations used in the differential equation solvers are dimensionless, only the change in angle and the damping changed the results from one run to another.

Several cables were examined, and small differences in results came about mainly from changes in cable inclination. The analysis of one of these is presented here. The cable is similar to the longest stay of the cable-stayed Second Severn Crossing Bridge, UK, and will be referred to as cable A. Cable A has a length of 244.4 m, a steel cross-sectional area of 11,250 mm^2 and an angle of inclination of 20.3°. The cable's structural damping has been estimated by Macdonald [20], from on-site measurements, to be about 0.05% and its mass per unit length 123.24 kg/m. A typical cable stay will have a damping value of about 0.1% [20,21]. The modulus of elasticity of the cable is $E = 1.95 \times 10^5\, N/mm^2$.

To suit future laboratory experiments, these quantities were scaled-down by a ratio of 1:114. All of the structural quantities are scaled with this factor, except for the mass per unit length quantities, which are scaled so that the example cable under examination has the same frequencies as those of the scaled bridge. The scaled quantities were not used in the cable's nonlinear equations of motion, as the equations are nondimensional, but were used for the finite element analyses. Also, for the prototype cable, the total static tension was estimated to be about 30% of yielding [20]. This quantity is also scaled so that the total static tension in the scaled cable is again equal to 30% of that required for material yielding.

5. Time-varying sinusoidal support excitation

5.1. Regions of nonlinear response (regions of instability)

The derived equations, parameterised for cable A, were used to investigate regions of instability in the two-dimensional parameter space of excitation circular frequency Ω and a parameter β, which is a function of the vertical support excitation amplitude Δ_{max}. The third dimension of the parameter space is the cable's maximum amplitude of vibration

$$\beta = \left(\frac{5\pi\sqrt{EA/\mu}}{\omega_1}\right)\left(\frac{\Delta_{max}}{l^2}\right). \tag{53}$$

Parameter β is scaled in order to be equal to 1.0 when $\Delta_{max} \cong 1.0$ m.

Bridge cable-stays are not only subject to their own structural damping but also to aerodynamic damping. The aerodynamic damping of cables varies with wind velocity. According to Virlogeux [21], when a cable is moving parallel to the wind, its aerodynamic damping can be found from the following equation:

$$\xi_{pk} = \rho V D C_d / 2\mu\omega_k, \tag{54}$$

where ρ is the air density (1.225 kg/m^3), V the wind velocity, C_d the drag coefficient, D =cable diameter, and ω_k the cable's modal frequencies.

When the cable is moving normal to the direction of the wind, then

$$\xi_{nk} = \rho V D C_d / 4\mu\omega_k. \tag{55}$$

A drag coefficient of C_d =1.2 [20], for cable A (cable diameter is 0.25 m), is equivalent to the drag that the cable will have with a wind speed of about 5 m s^{-1}. Table 1 shows the damping values found using these parameters and Eqs. (54) and (55).

Macdonald [20] estimated damping values for a cable with similar characteristics to cable A, from on-site measurements, and found that the cable's actual, normal to wind, damping ξ_{n1} was near 0.0015. This value is close to that found theoretically (0.00155) from Eq. (54) and this, together with the cable's structural damping of 0.05%, was used as the damping value for a second analysis. The remaining modal damping values were calculated as multiples of this value. With this increase in damping, only small differences in the cable's behaviour were observed. Consequently, a much higher damping value for cable A was chosen for a third analysis, in order to examine the effects that a large damping value would have on the dynamics of the cable. By considering extreme changes in the parameters that govern the aerodynamic damping of the cable, a larger cable damping value was found. The drag coefficient was increased from C_d =1.2 to $C_d = 2.1$, for a wind velocity of 30 m s^{-1}, even though this is highly unlikely as C_d drops from C_d =1.2 to C_d =0.4 after a wind velocity of about 10 m s^{-1}. This may, of course, be applicable if rain rivulet diffusers are placed around a cable. Revised, increased damping values are also shown in Table 1. The implementation of both low and high damping values was achieved using Eqs. (49) and (50).

Table 1
Theoritical ξ damping values for cable A, modes 1–4

	ξ_p when cable velocity parallel to wind	ξ_n when cable velocity normal to wind
Low damping		
First mode	0.00310	0.00155
Second mode	0.00155	0.00078
Third mode	0.00103	0.00517
Fourth mode	0.00078	0.00388
High damping		
First mode	0.0325	0.0163
Second mode	0.0163	0.00825
Third mode	0.01083	0.00902
Fourth mode	0.00813	0.00406

When solving the system of differential equations, which is represented by Eqs. (47) and (48), it becomes clear that the results are in the form of generalised nondimensional coordinates. These must be multiplied by the appropriate shape functions for a displacement to be found at some point along the length of the cable. The calculation of absolute maximum cable displacements is slightly more complicated. The methodology, although, is fairly straightforward.

As in other mechanical systems, maximum and minimum displacements can be calculated by equating the first derivative of the cables' displacement equations to *zero*, i.e. the velocity of the system is *zero*. Similarly, by replacing the results, as obtained from the solution of the system of Eqs. of (47) and (48), into Eqs. (36) and (37), finding the first derivative (with respect to time) of Eqs. (36) and (37) and by equating those expressions to *zero*, the locations of maximum and minimum cable displacements can be calculated. Once the locations have been found, actual displacements can be calculated and the maximum of those can be selected. Note that the maximum displacements, as calculated when following this procedure, will include deck displacements. If one wishes to acquire pure cable displacements, then the deck displacements must be subtracted from these.

Four separate three-dimensional graphs, which show clear regions of large amplitude cable vibrations, were created for cable A. The zones of large displacement from the two analyses of cable A, using the derived nonlinear equations of motion of the cable, are presented in Figs. 4a–d, with the parameters used in each analysis stated. Fig. 4a represents the variation of maximum in-plane cable displacements with structural damping of 0.05%. Fig. 4b shows the variation of the maximum out-of-plane displacements with structural damping. Fig. 4c shows the variation of the maximum in-plane cable displacements with structural and aerodynamic damping (3.3%), while Fig. 4d shows the variation of the maximum out-of-plane displacements with structural and aerodynamic damping. The displacements in Figs. 4a–d represent maximum cable displacements at any location along the cable. In most large amplitude response regions, maximum and steady-state displacements coincided. The analyses were performed using four in-plane and out-of-plane shape functions. The reasons for this are explained in the following section.

As can clearly be seen from Figs. 4a–d, regions of large amplitude cable vibrations are found from the multiple shape-function analyses at excitation frequencies $\Omega = 0.5 \cdot \omega_1^{\mathrm{nl}}$ and $\Omega = 1.3 \cdot \omega_1^{\mathrm{nl}}$. These regions, which cannot be found through single shape-function analysis, have been verified through finite element analysis using SOLVIA. Both gradually increasing transient sinusoidal time-histories and abrupt transient sinusoidal time-histories were examined. It is important to note that displacement amplitudes are significant, especially for the higher amplitude cable end excitations. The amplitudes found were in the region of $\sim 0.0l \rightarrow 0.022l$, i.e. the maximum displacement of the example prototype cable, in this parameter region, would be 10.75 m from peak-to-peak. Multiple cable analyses, using multiple shape-functions, showed that 'cable stiffening' occurs for very large amplitude vibrations, and that large amplitude out-of-plane cable vibrations can contribute greatly to this phenomenon. This is discussed in detail in a following section.

5.2. Multiple shape function analyses

Several nonlinear analyses of the cables, using one or multiple shape functions, were made and compared with results obtained from nonlinear finite element analyses. The nonlinear finite

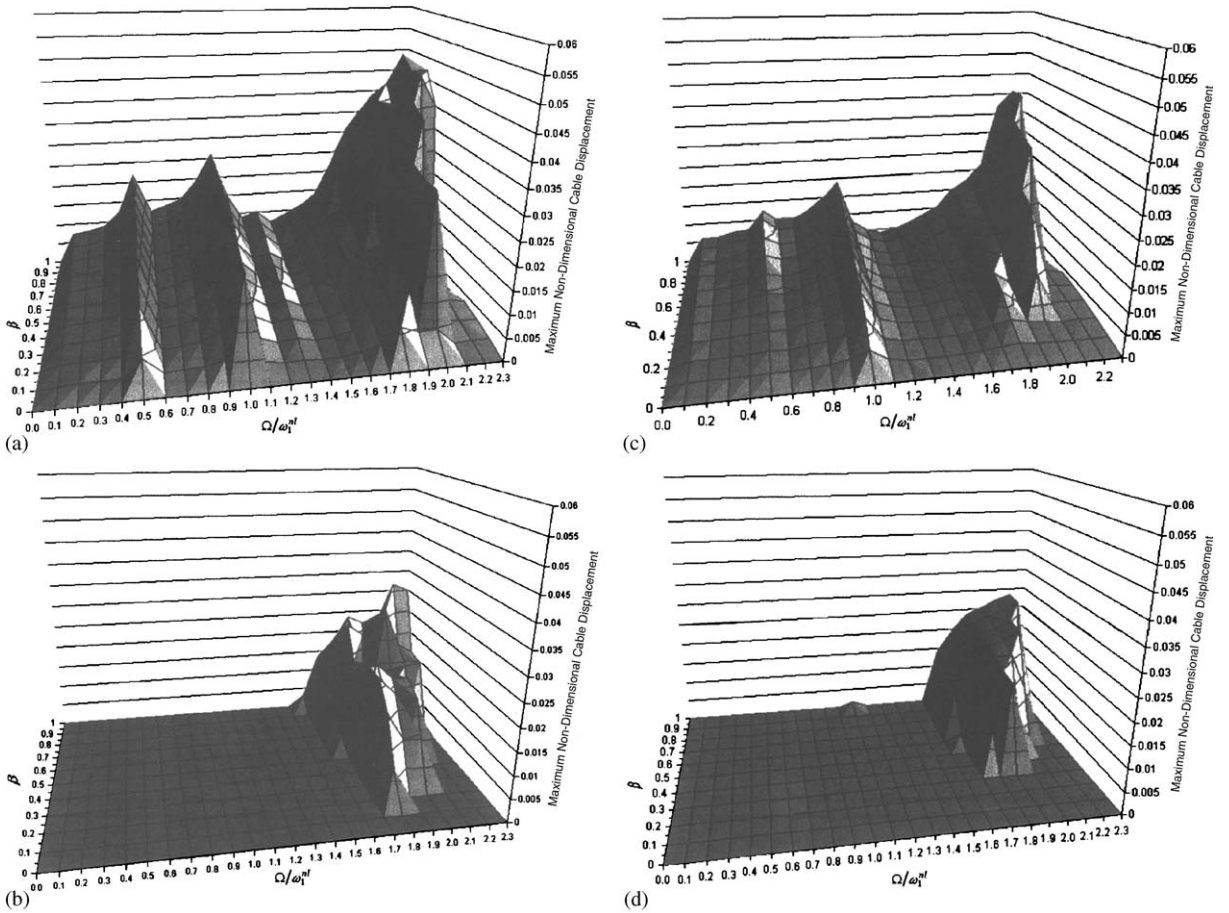

Fig. 4. (a) Maximum in-plane nondimensional displacement for a cable with $\theta = 20.3^\circ$, $\xi = 0.05\%$. (b) Maximum out-of-plane nondimensional displacement of a cable with $\theta = 20.3^\circ$, $\xi = 0.05\%$. (c) Maximum in-plane nondimensional displacement of a cable with $\theta = 20.3^\circ$, $\xi = 3.3\%$. (d) Maximum out-of-plane nondimensional displacements of a cable with $\theta = 20.3^\circ$, $\xi = 3.3\%$.

element analysis was performed using a multi-truss element cable that was pin-jointed at both ends. Single shape-function numerical analyses produced time history results that were in very good agreement with those found from finite element analyses, but only for low-frequency and low-amplitude support excitations. When the excitation frequency and amplitude was increased, the resultant displacement time-histories were significantly different from those found using finite element analysis. In-plane cable displacements include the static load offset. (see Figs. 5a–e).

Fig. 5a represents the in-plane displacement time-history for the example cable with 1% damping at a distance $x = 0.4\,l$ along the length of the cable. The support excitation amplitude is 0.009627 m, with a circular frequency of $\Omega = 1.7\omega_1^{\mathrm{nl}}$ or 6.59 rad/s. The analysis is nonlinear and performed using SOLVIA. Fig. 5b represents the out-of-plane displacement time-history of the same cable at distance $x = 0.5l$ (mid-span). Figs. 5c and d are equivalent to Figs. 5a and b, only that here the displacement time-histories were calculated using the predefined nonlinear equations

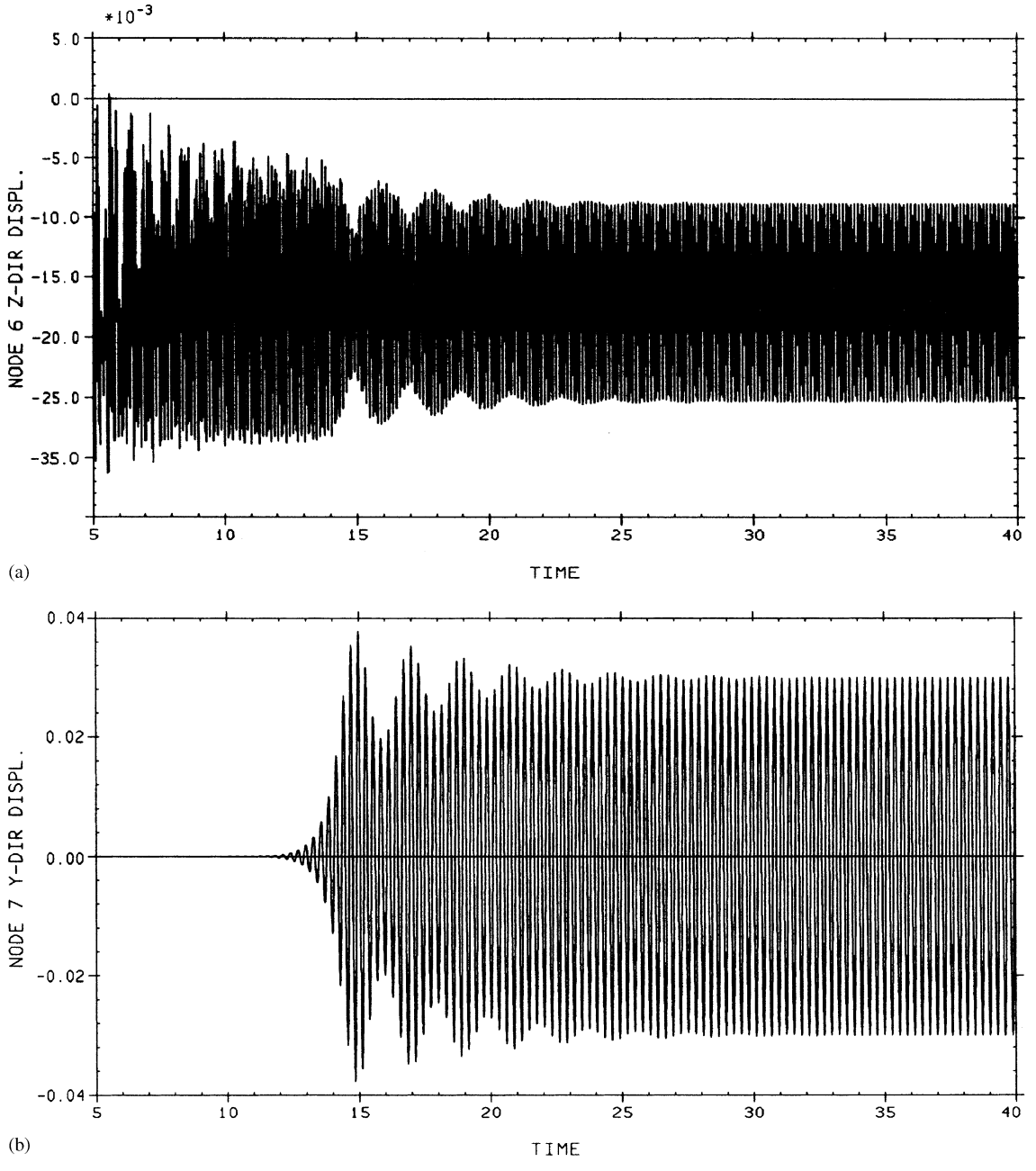

Fig. 5. (a) In-plane displacement of cable A at position $x=0.4\,l$, found using SOLVIA, $\Omega = 1.7\omega_1^{nl}$, $\beta = 0.01$, $\xi = 1\%$. (b) Out-of-plane displacement of cable A at $x=0.5\,l$, found using SOLVIA, $\Omega = 1.7\omega_1^{nl}$, $\beta = 0.01$, $\xi = 1\%$. (c) In-plane displacement of cable A at position $x=0.4\,l$, found using four shape-functions and Dsolver, $\Omega = 1.7\omega_1^{nl}$, $\beta = 0.01$, $\xi = 1\%$ (3 s time-base difference to SOLVIA). (d) Out-of-plane displacement of a cable A at $x=0.5\,l$, found using four shape-functions and Dsolver, $\Omega = 1.7\omega_1^{nl}$, $\beta = 0.01$, $\xi = 1\%$ (3 s time-base difference to SOLVIA). (e) In-plane displacement of cable A at position $x=0.4\,l$, using one shape-functions and Dsolver, $\Omega = 1.7\omega_1^{nl}$, $\beta = 0.01$, $\xi = 1\%$. (f) Example Lyapunov exponent for cable a with $\Omega/\omega_1^{nl} = 2.5$, $\beta = 1.0$.

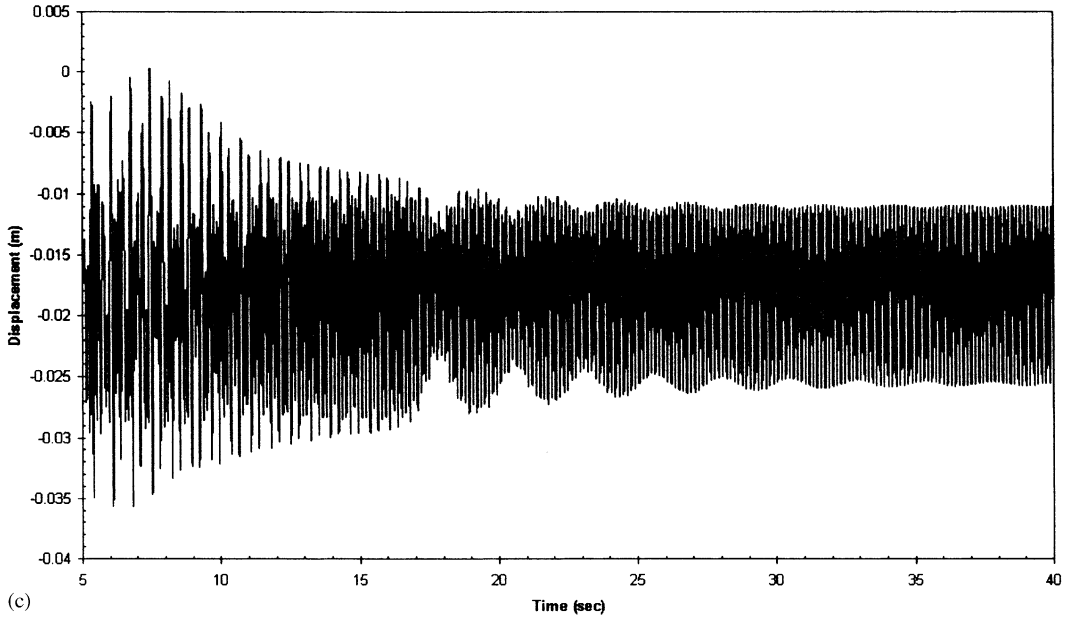

(c)

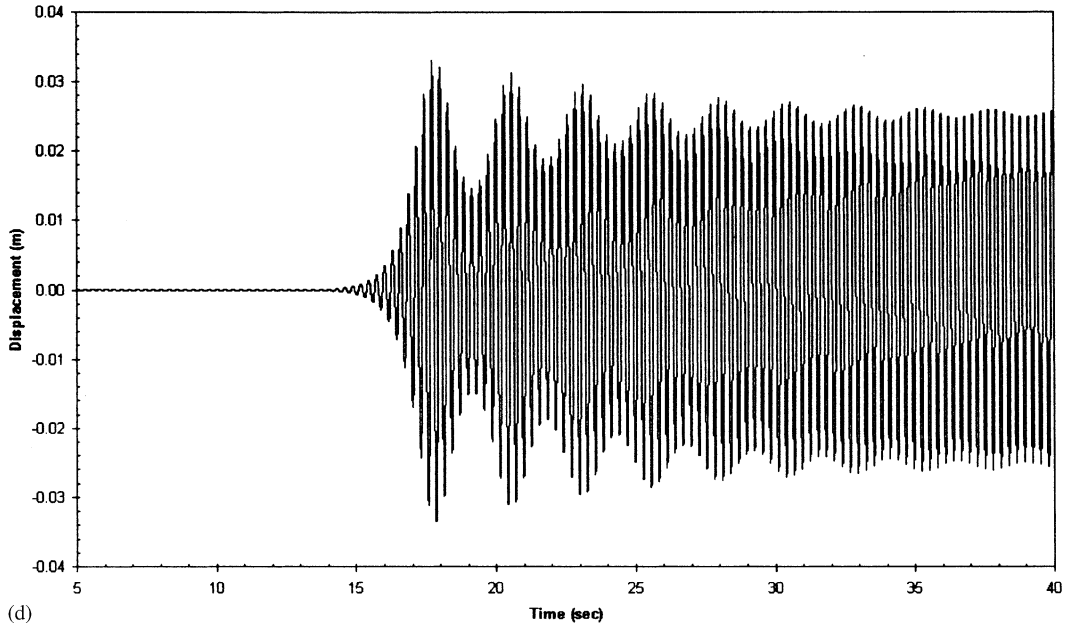

(d)

Fig. 5. (*Continued*)

of motion that have been numerically integrated using DSolver. In this analysis, *four* shape functions were used. Fig. 5e represents the same analysis as that performed in Fig. 5c except that only *one* shape function was used. It is clear when comparing the time-histories of Figs. 5a, c and e that the displacement time-history found using only *one* shape function gave a significantly

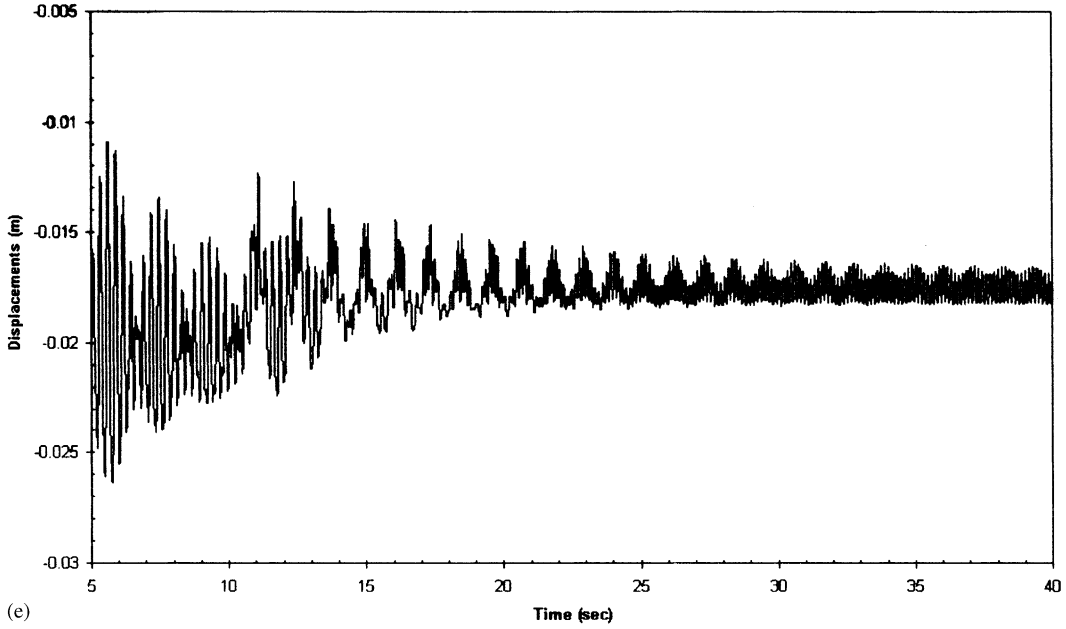

(e)

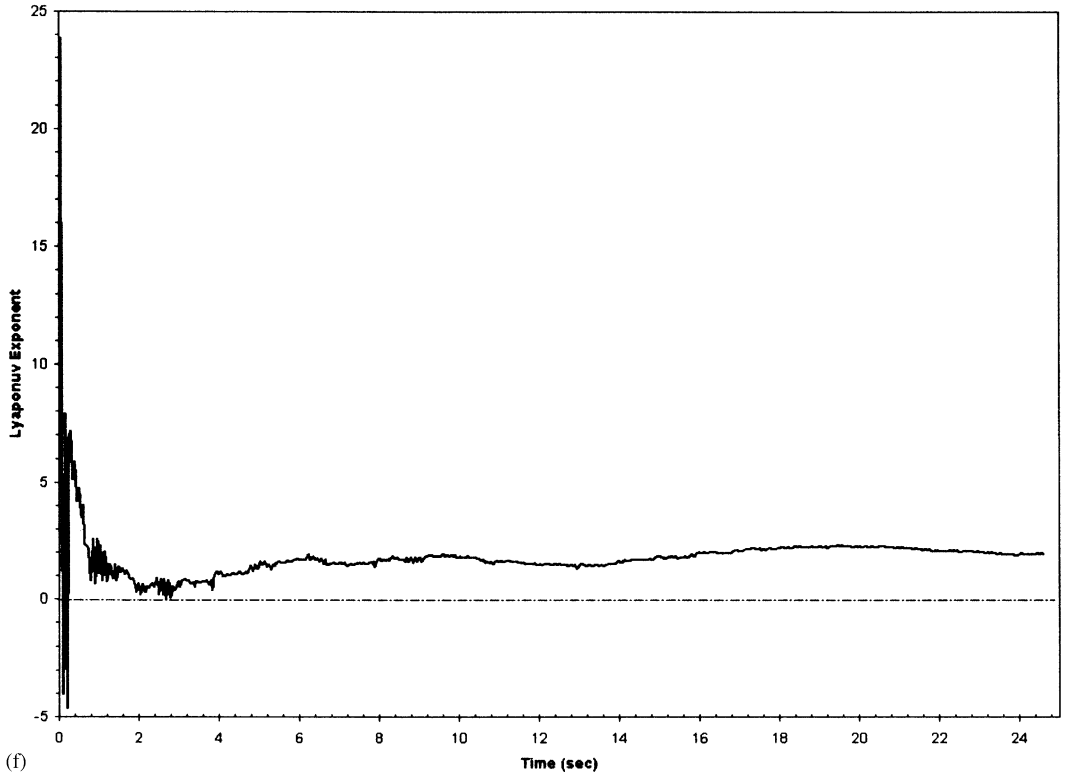

(f)

Fig. 5. (*Continued*)

inaccurate result, while those found using *four* shape functions were in good agreement with those calculated through finite element analysis.

5.3. Periodic, quasi-periodic and chaotic sub-regions

Figs. 4a–d illustrate the maximum expected in-plane and out-of-plane nondimensional displacements of cable A for varying support excitation amplitudes and frequencies, but they do not give a clear picture of whether the displacement time histories are chaotic, periodic or quasi-periodic. For this reason, Figs. 4a and b have been replicated in Figs. 6a and c using 2-dimensions and lines of equal amplitude to represent the various displacement amplitudes. Figs. 6b and d show periodic, quasi-periodic and chaotic regions corresponding to Figs. 6a and c, respectively. These have been determined by computing the Lyapunov Exponent (Fig. 5f) of the time-histories of cable A, assuming standard damping of 0.05% and excited under various frequencies and amplitudes. According to Moon [22], when the Lyapunov Exponent is negative then the time-history is periodic. Similarly, when it is positive it is chaotic. In this analysis, it was found that very small positive values represented quasi-periodic motion. The algorithm that was used for this computation was that of Wolf et al. [23]. The Lyaponuv Exponent was calculated over a time-history with a length of over 120 s, to make sure that it was not being calculated within a transient region. Note that the regions will change as the damping of the cable and its angle of inclination change. For higher levels of damping, e.g. cable A with 3.3% damping, it was found that the cable will displace periodically in all regions, both in-plane and out-of-plane, after an initial transient phase.

5.4. Change of initial conditions

The previous analyses assumed that the cable's vibrations start from a static or near static position. This may be true for many cases, but not for all. For this reason, another analysis of cable A, once again only assuming structural damping of 0.05%, was undertaken to examine the effect of a change in the cable's initial conditions. An initial mid-span in-plane prototype cable velocity of $0.25\,\mathrm{m\,s^{-1}}$ was chosen, as this value is typical of the measured response on the actual cable-stayed bridge. This value has been scaled and nondimensionalised so that it can be used as a general value for any similar cable.

Figs. 7a and b show the effect that an initial condition can have on the vibrations of a cable. Total in-plane displacement levels increased by 10–20%, within most of the regions of large amplitude vibration, when compared to Figs. 4a and 6a. Amplitudes at $\Omega = 1.3\omega_1$ remained the same, whilst amplitudes around $\Omega = 1.3\omega_1$ increased slightly.

In this example, the energy, which is transferred from the support to cable through the displacement of the support, is compounded by the initial stored and kinetic energy imposed on the system by the $0.25\,\mathrm{m\,s^{-1}}$ initial cable velocity. The new total system energy acts in such a way as to increase the cable's maximum in-plane displacement levels by 10–20%, as previously mentioned. Thus, any positive energy imposed on the system by a *non-zero* initial condition, either in the cable or the supporting structure, may act in such a way as to increase the total displacement amplitudes of the cable. The comparison, of course, must be made between two identical support excitations, with and without a positive amount of initial energy.

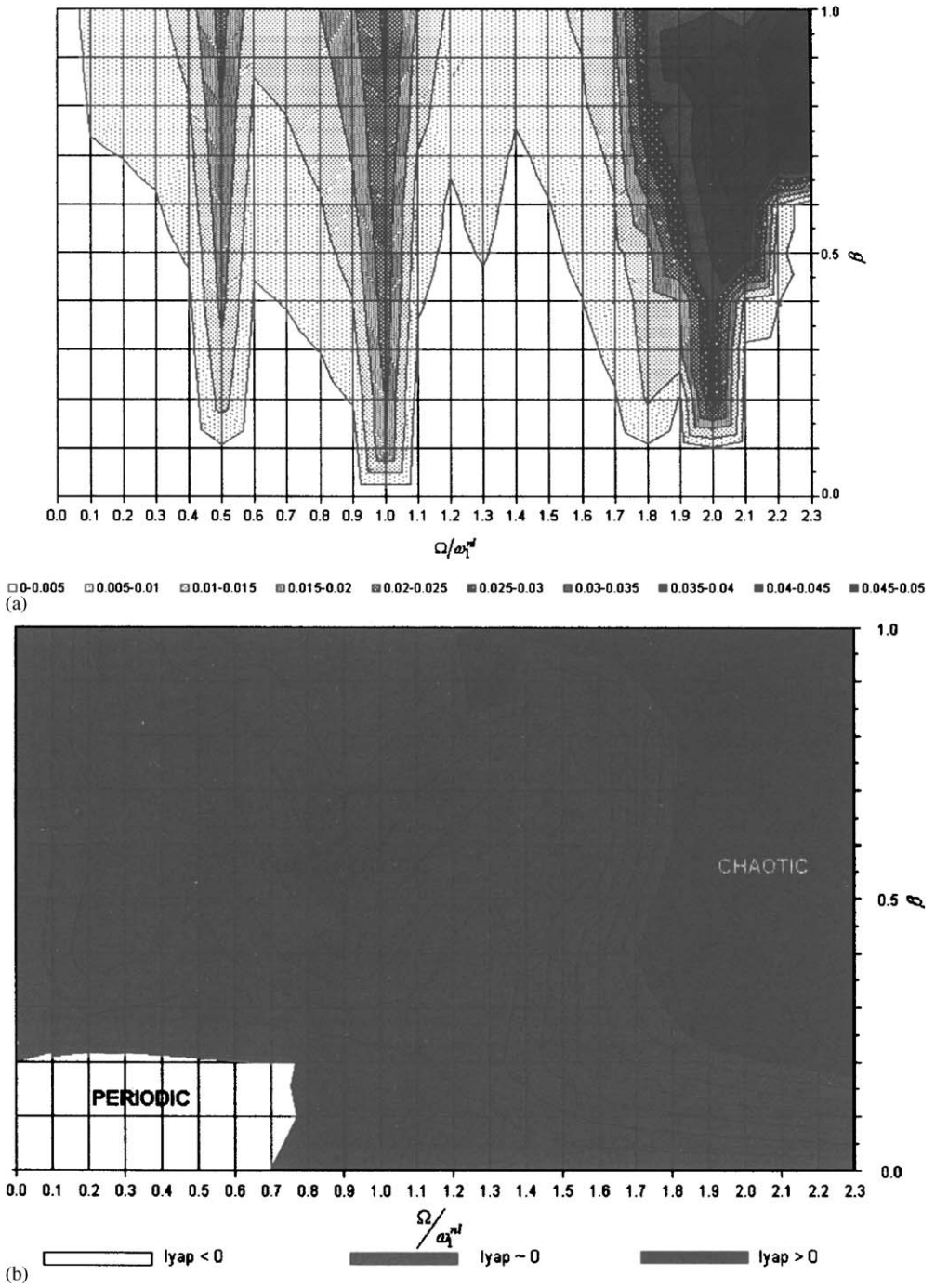

Fig. 6. (a) Maximum in-plane nondimensional cable displacements of a cable with $\theta = 20.3^\circ$, $\xi = 0.05\%$. (b) In-plane periodic, quasi-periodic and chaotic regions of a cable with $\theta = 20.3^\circ$, $\xi = 0.05\%$. (c) Maximum out-of-plane non-dimensional displacements of a cable with $\theta = 20.3^\circ$, $\xi = 0.05\%$. (d) Out-of-plane periodic and chaotic regions of a cable with $\theta = 20.3^\circ$, $\xi = 0.05\%$.

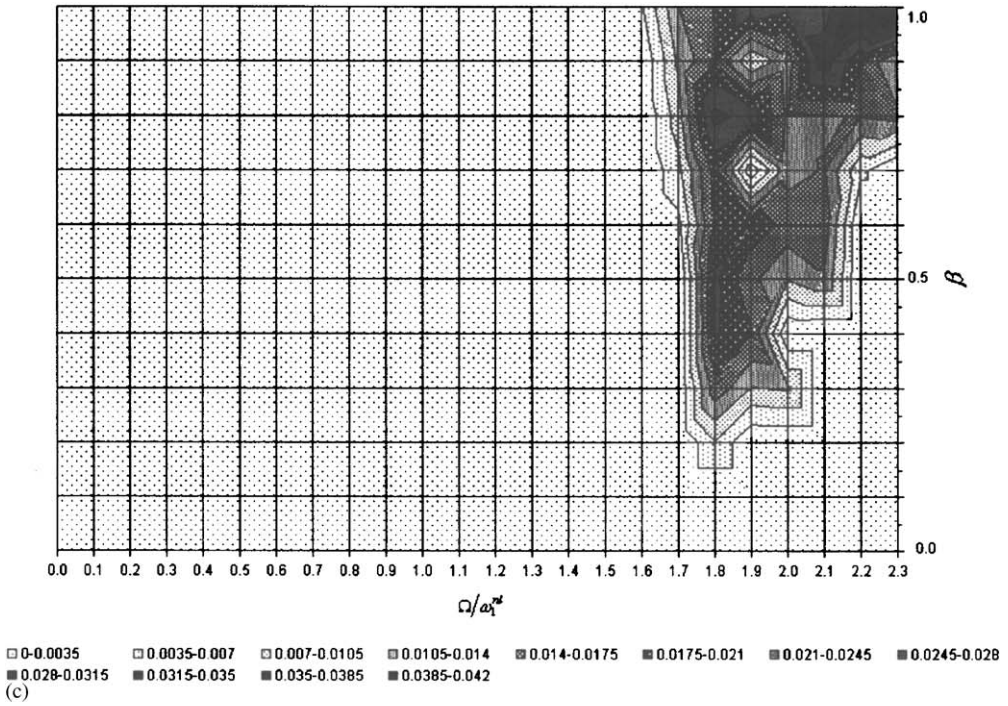

(c)

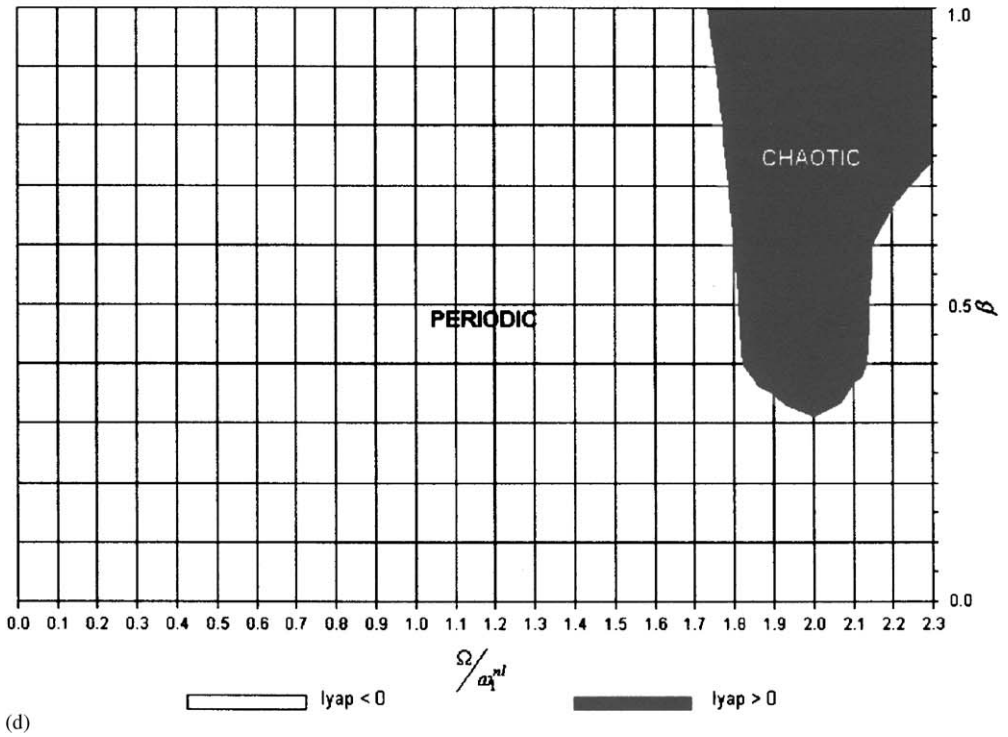

(d)

Fig. 6. (*Continued*)

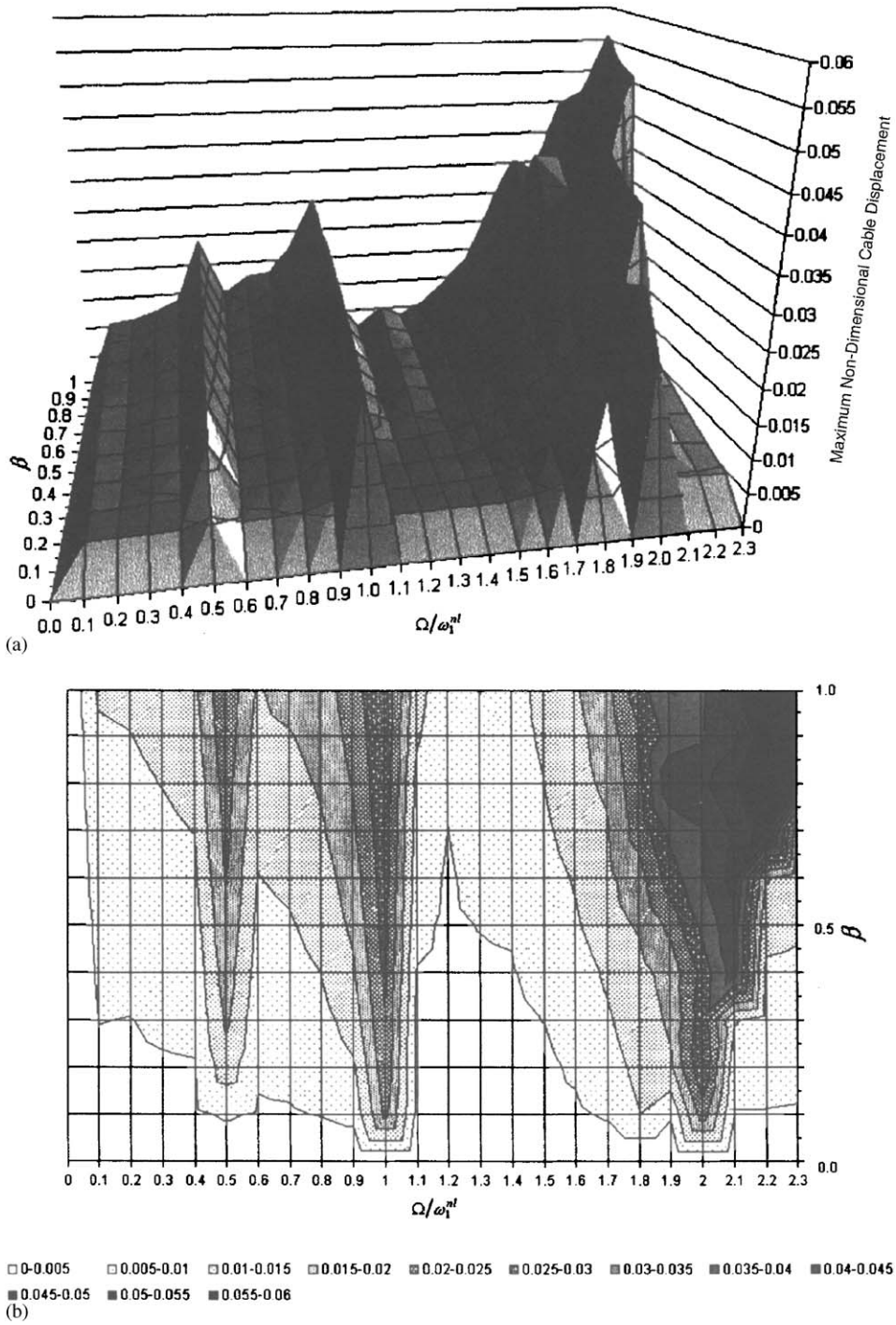

Fig. 7. (a) Maximum in-plane nondimensional displacements for a cable with an intial in plane cable velocity of $v = 0.25\,\mathrm{m\,s^{-1}}$ and $\theta = 20.3^{\circ}$, $\xi = 0.05\%$. (b) Maximum in-plane nondimensional displacements for a cable with an initial in-plane cable velocity of $v = 0.25\,\mathrm{m\,s^{-1}}$ and $\theta = 20.3^{\circ}$, $\xi = 0.05\%$.

Out-of-plane vibrations were also examined. It was found that because out-of-plane displacements increase gradually, a change in initial conditions does not influence the cable's maximum out-of plane response. The initial positive energy imposed on the system, by a *non-zero* initial condition, is dissipated or distributed over a large number of cycles, thus offering little as an effect on the large amplitude out-of-plane cable displacement amplitudes.

6. Cable stiffening

As stated in Section 5.1, the cable acts as a nonlinear stiffening spring at higher amplitude cable vibrations. This can be understood by examining Figs. 8a and b. They show the stiffening effect for a cable with 0.05% and 3.3% damping, respectively. For the lower frequency segments of the parameter plane, the cable does not stiffen with increasing amplitudes of excitation. This is not true, although, for the higher frequencies ($\Omega > 2.0\omega_1^{nl}$), where cable displacement amplitudes are greatest. In this area, the cable stiffens significantly, inducing changes in its own natural frequencies. The higher amplitude vibrations were observed at excitation frequencies other than those that had already been theoretically predetermined. The cable stiffening effect is greatly increased in the region of $\Omega > 2.0\omega_1^{nl}$ by the out-of-plane cable vibrations. Out-of-plane vibrations work in conjunction with the in-plane vibrations, increasing the tension of the cable and consequently increasing the stiffening effect. It is known that the tension of an excited cable varies in time and that a cable will behave similar to a nonlinear stiffening spring, as described by Duffing's equation [6]. Here it is shown that increases in a cable's tension must be significant for a change in the cable's natural frequency. The particular cable-stiffening effect is believed to be studied for the first time here.

In none of the analyses did cable A's longitudinal axial stress ever reach that required for yielding. The maximum axial-load achieved during the analysis was a scaled axial load of $N_c = 290$ N. This equates to a prototype maximum stress of $\sigma_{max} = 1430$ MPa, which compares with a yield stress of $\sigma_y = 1500$ MPa.

7. Low level cable support excitation

Throughout the analyses, the response of a cable, to relatively high levels of cable support excitation, were examined. To determine the effects that a low-level cable support excitation might have on the response of a cable, the responses of cable A, at various frequencies with $\beta = 0.01$ and with two different levels of damping (0.05% and 3.3%), were calculated. They are presented in Fig. 9. As can be seen from Fig. 9, the cable can exhibit very large in-plane displacements even for the very small parameter value of $\beta = 0.01$. At $\Omega = 1.0\omega_1^{nl}$ and $\Omega \approx 1.8\omega_1^{nl}$, cable displacements to cable support displacements were at a ratio of 259.74:1 and 45.45:1, respectively, i.e. if the prototype cable with 0.05% damping were to receive a 0.01 m support displacement at $\Omega = 1.0\omega_1^{nl}$, the total expected in-plane cable displacements would be 2.59 m. These displacement levels are drastically reduced with the introduction of the higher level of damping and are not due to the nonlinearity of the cable, i.e they could have been found by performing a simple linear analysis.

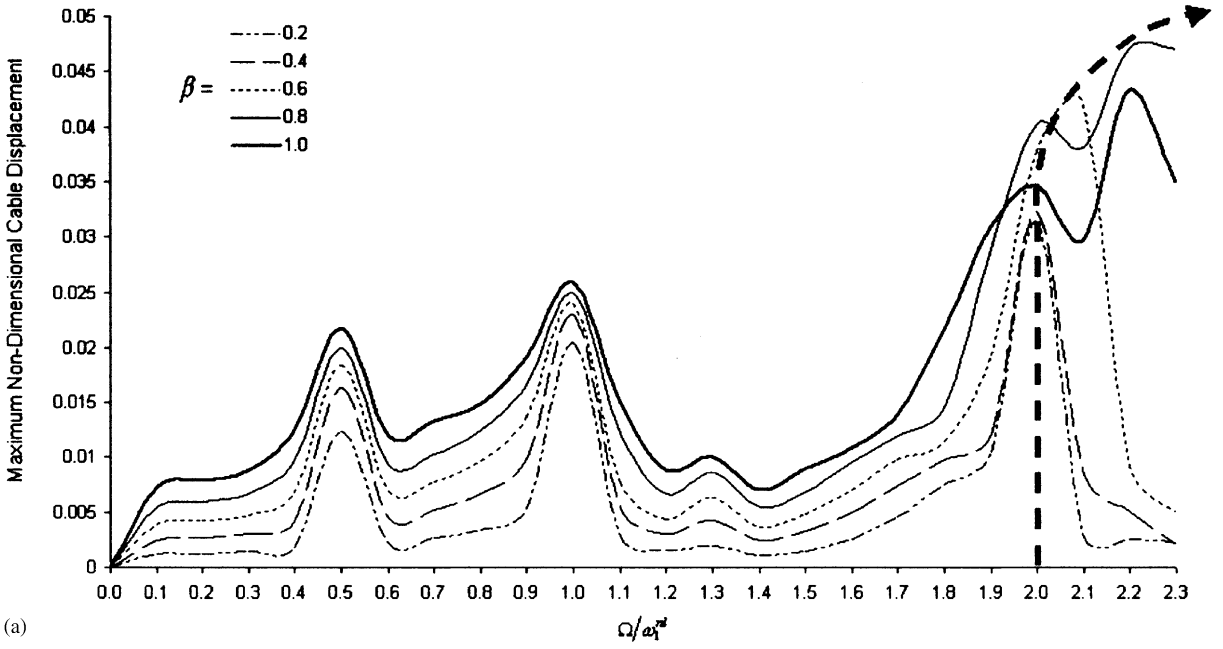

(a)

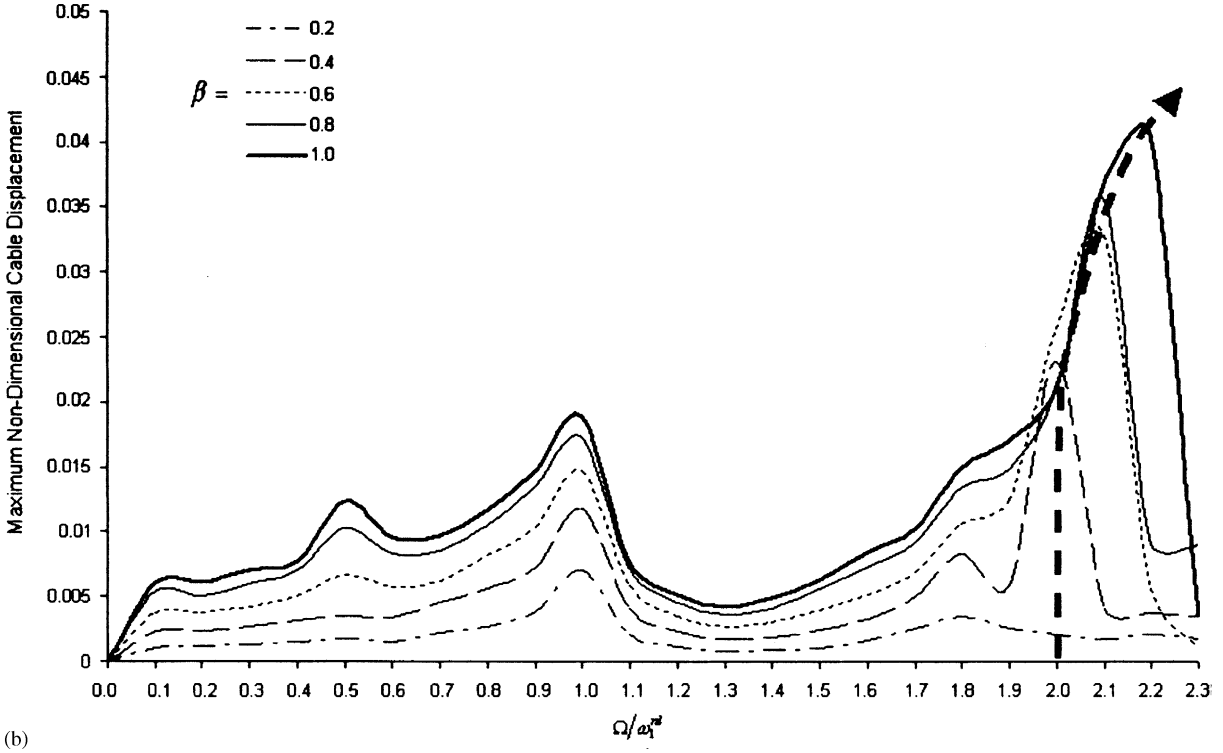

(b)

Fig. 8. (a) Large amplitude stiffening effect of a cable with $\theta = 20.3°$, $\xi = 0.05\%$. (b) Large amplitude stiffening effect of a cable with $\theta = 20.3°$, $\xi = 3.3\%$.

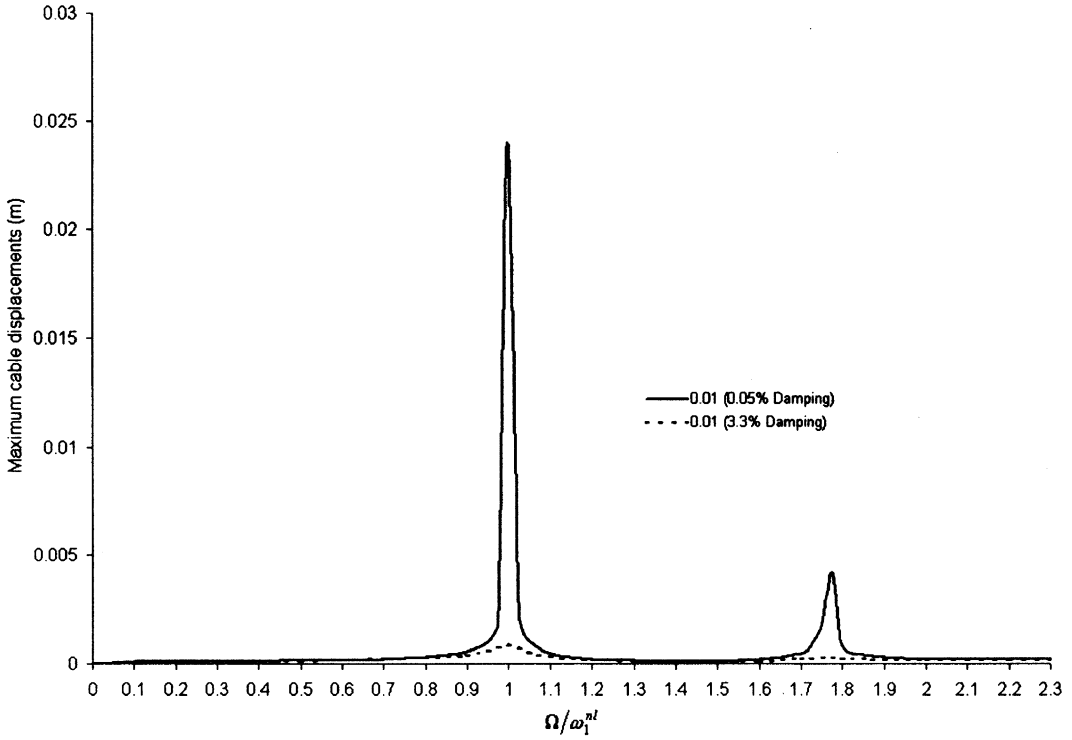

Fig. 9. In-plane cable response to low-level sinusoidal support excitation with $\beta = 0.01$, $\xi = 0.05\%$ & 3.3%, $\theta = 20.3^{\circ}$.

8. Concluding remarks

In this paper, the nonlinear differential equations of motion for a hanging cable have been reformulated and presented in a manner that makes their implementation in numerical integration packages straightforward. This in turn makes the sinusoidal parametric study of individual cables or groups of cables much less time-consuming and laborious. It has been shown that large amplitude in-plane cable vibrations are not confined to excitation circular frequencies of $\Omega = 1.0\omega_1^{\mathrm{nl}}$ and $\Omega = 2.0\omega_1^{\mathrm{nl}}$ as previously assumed when examining the parameter range $\Omega : 0\omega_1^{\mathrm{nl}} \rightarrow 2.3\omega_1^{\mathrm{nl}}$. Large amplitude cable vibrations may also occur at other excitation circular frequencies, e.g. $\Omega = 0.5\omega_1^{\mathrm{nl}}$ and $\Omega = 1.3\omega_1^{\mathrm{nl}}$. The response at these excitation frequencies is significant and should not be ignored during cable structural design.

Nonlinear differential equations of motion of hanging cables provide a quick and convenient tool for cable vibration analysis. It is important, though, that the appropriate number of shape-functions is used when calculating cable response, through numerical integration of ODEs. The use of too few shape functions will hinder the location of important regions of large amplitude cable vibrations and, at higher frequencies, grossly under-estimate the total cable response.

Cable stiffening occurs for large amplitude in-plane and out-of-plane cable vibrations. This can be seen as a shift in the main region of parameter instability, from lower to higher frequencies, both in-plane and out-of-plane. Out-of-plane cable vibrations contribute greatly to this phenomenon, as they increase total cable tension.

The support excitation amplitude required, to induce large amplitude cable vibrations, increases with increasing levels of damping. As such, cable damping is an important factor in the creation of large-amplitude cable-vibration or unstable zones in the parameter plane. The structural designer or researcher, although, must bear in mind that large amplitude structural vibrations do not always go hand-in-hand with very large wind velocities. Even when cable damping is relatively high, the cable response within unstable regions does not differ greatly to that found within unstable regions of lower damped cables.

Cables, even for relatively low levels of damping, will, on the whole, behave periodically or quasi-periodically. They may, although, behave chaotically, both in-plane and out-of-plane, for higher frequency and larger amplitude excitations. This is especially true when cable damping levels are low.

Various assumptions for expected initial cable conditions must be made when examining cable vibrations, as a *non-zero* initial condition may have the effect of increasing the maximum total cable displacements by a significant amount. Cable displacements increased by an average of 15%, when examining the cable's dynamic response to a arbitrarily selected—but realistic—initial in-plane cable velocity of 0.25 m/s.

Transient phases in the examination of cable displacement time-histories are important, as in-plane instabilities tend to occur very quickly after support excitations are applied. They are not so important for the examination of out-of-plane instabilities. Gradual sinusoidal support excitation transients only have the effect of delaying the onset of instabilities, not preventing them.

It has been shown that even for very low levels of cable excitation at particular excitation frequencies, the amplitude of a cable's in-plane displacements, when cable damping is low, may be hundreds of times greater than the amplitude of its support displacements. If the avoidance of coinciding excitation and cable frequencies is not possible, special attention must be given to passive damping mechanisms or, if appropriate, vibrational control through active or semi-active means.

Finally, it is important to note that the effects of cable-deck interaction were not considered during this work. The effects of this interaction are examined in greater detail in a subsequent paper. The effects of stochastic support excitation are examined in Part 2 of this paper [24].

Appendix A

A.1. Definition of coefficients for Eqs. (42), (43) and (44)

$$a_{1i} = -v_l^2(\pi i)^2,$$

$$a_{2i} = \frac{2}{(\pi i)^2}(1 - \cos \pi i)^2,$$

$$a_{3i} = \frac{2}{i\pi}(1 - \cos i\pi),$$

$$\beta_1 = -2v_l^2 c \cos \theta,$$

$$\beta_2 = -4v_l^2 \cos^2\theta,$$

$$\beta_3 = -cv_l^2,$$

$$\beta_4 = \beta_1,$$

$$\beta_5 = \tfrac{1}{2}v_l^2(\pi i)(1-\cos i\pi)\cos\theta,$$

$$\beta_{6i} = \frac{c}{4}(\pi i)v_l^2(1-\cos i\pi),$$

$$\beta_{7i} = \beta_{5i},$$

$$\beta_{8i} = \beta_{6i},$$

$$\gamma_1 = 2v_t^2\cos\theta,$$

$$\gamma_2 = cv_l^2\sin\theta,$$

$$\gamma_3 = -\frac{c^2}{3}v_l^2\cos\theta,$$

$$\gamma_4 = \tfrac{2}{3}cv_l^2\cos^2\theta,$$

$$\gamma_5 = 2v_l^2\cos\theta\sin\theta,$$

$$\lambda_{1i} = -v_l^2(\pi i)^2,$$

$$\gamma_6 = -\frac{2c}{3}v_l^2\cos^2\theta,$$

$$\gamma_7 = \tfrac{4}{3}v_l^2\cos^3\theta,$$

$$\gamma_{8\bar{x}} = \left\{\frac{2}{i\pi} - \frac{2}{(i\pi)^3}(1-\cos i\pi)\right\}\cos\theta,$$

$$\tau_1 = \left(\sin\theta - \frac{c}{3}\cos\theta\right),$$

$$\tau_2 = -c,$$

$$\tau_3 = \tfrac{1}{4},$$

$$\tau_4 = \tfrac{2}{3}\cos^2\theta,$$

$$\tau_5 = -2\cos\theta.$$

References

[1] A.G. Davenport, A simple representation of the dynamics of a massive stay cable in the wind, *Proceedings of the International Conference of Cable-Stayed and Suspension Bridges (AFPC)*, Vol. 2, Deauville, 1994, pp. 427–438.

[2] C. Verwiebe, Rain–Wind induced vibrations of cables and bars, in: A. Larsen, S. Esdahl (Eds.), *Bridge Aerodynamics*, Balkema, Rotterdam, 1998, pp. 255–263.

[3] M. Matsumoto, N. Shiraishi, H. Shirato, Rain–Wind induced vibration of cables of cable-stayed bridges, *Proceedings of the Eighth International Conference on Wind Engineering*, London, Canada, 1991.
[4] M. Masumoto, Observed behaviour of prototype cable vibration and its generation mechanism, in: A. Larsen, S. Esdahl (Eds.), *Bridge Aerodynamics*, Balkema, Rotterdam, 1998.
[5] H. Yamaguchi, Y. Fujino, Stayed cable dynamics and its vibration control, in: A. Larsen, S. Esdahl (Eds.), *Bridge Aerodynamics*, Balkema, Rotterdam, 1998, pp. 235–255.
[6] H.M. Irvine, T.K. Cauchey, The linear theory of free vibrations of a suspended cable, *Proceedings of the Royal Society of London A* 341 (1974) 299–315.
[7] N.M. Irvine, *Cable Structures*, MIT Press, Cambridge, MA, 1981.
[8] K. Takahashi, Y. Konishi, Non-linear vibrations of cables in three dimensions—Part I: non-linear free vibrations, *Journal of Sound and Vibration* 118 (1) (1987) 69–84.
[9] K. Takahashi, Y. Konishi, Non-linear vibrations of cables in three dimensions—Part II: out-of-plane vibrations under in-plane sinusoidally time-varying load, *Journal of Sound and Vibration* 118 (1) (1987) 85–97.
[10] Y. Fujino, P. Warnitchai, B.M. Pacheco, An experimental and analytical study of autoparametric resonance in a 3DOF model of a cable-stayed-beam, *Nonlinear Dynamics* 4 (1993) 111–138.
[11] P. Warnitchai, Y. Fugino, T. Susumpow, A non-linear dynamic model for cables and its application to a cable-structure system, *Journal of Sound and Vibration* 187 (4) (1995) 695–712.
[12] J.L. Lilien, A. Pinto da Costa, Vibration amplitudes caused by parametric excitation of cable stayed structures, *Journal of Sound and Vibration* 174 (1) (1994) 69–90.
[13] A. Pinto da Costa, J.A.C. Martins, F. Branco, J.L. Lilien, Oscillations of bridge stay cables induced by periodic motions of deck and/or towers, *Journal of Engineering Mechanics* 122 (1996) 613–622.
[14] N.C. Perkins, Modal interactions in the non-linear response of elastic cables under parametric external excitation, *International Journal of Non-Linear Mechanics* 27 (2) (1992) 233–250.
[15] R. Uhrig, On kinetic response of cables-stayed bridges due to combined parametric and forced excitation, *Journal of Sound and Vibration* 165 (1) (1993) 185–192.
[16] J.M. Aquirregabiria, Dsolver—Dynamic numerical integration, 1992–1998, http://tp.lc.ehu.es/jma.html.
[17] C.T. Georgakis, Non-linear Dynamics of Cable Stays and Cable-Structure Interaction, PhD Thesis, Departments of Civil and Aerospace Engineering, University of Bristol, UK, 2001.
[18] H.E. Nusse, J.A. Yorke, *Dynamics: Numerical Explorations—Dynamics II*, second ed, Springer, New York, 1998.
[19] SOLVIA95—SOLVIA Finite Element System, SOLVIA Engineering AB, Trefasgatan 3, SE-721 Västerås, Sweden, July 1996.
[20] J.H.G. Macdonald, Identification of the Dynamic Behaviour of a Cable-Stayed Bridge from Full-Scale Testing during and after Construction, PhD Thesis, Department of Civil Engineering, University of Bristol, 2000.
[21] M. Virlogeux, Cable vibrations in cable-stayed bridges, in: A. Larsen, S. Esdahl (Eds.), *Bridge Aerodynamics*, Balkema, Rotterdam, 1998, pp. 213–233.
[22] F.C. Moon, *Chaotic and Fractal Dynamics: An Introduction for Applied Scientists and Engineers*, Wiley, New York, 1992.
[23] A. Wolf, J.B. Swift, H.L. Swinney, J.A. Vastano, Determining Lyapunov exponents from a time series, *Physica* 16D (1985) 285–317.
[24] C.T. Georgakis, C.A. Taylor, Nonlinear dynamics of cable stays. Part 2: stochastic support excitation, *Journal of Sound and Vibration* 281 (3–5) (2005) 565–591, this issue, doi:10.1016/j.jsv.2004.01.023.